Chemical Engineering Journal 191 (2012) 563–570

Contents lists available at SciVerse ScienceDirect

Chemical Engineering Journal

journal homepage: www.elsevier.com/locate/cej

# Cerium(IV) oxide: Synthesis in alkaline and acidic media, characterization and adsorption properties

Maximiliano Brigante*, Pablo C. Schulz

*INQUISUR, Departamento de Química, Universidad Nacional del Sur, Av. Alem 1253, (8000) Bahía Blanca, Argentina*

ARTICLE INFO

*Article history:*
Received 19 December 2011
Received in revised form 18 February 2012
Accepted 20 February 2012

*Keywords:*
Ceria
Synthesis
Cetyltrimethylammonium tosylate
Nanoparticles
Adsorption kinetics
Tetracycline-type antibiotics

ABSTRACT

Cerium(IV) oxide or ceria materials were synthesized in alkaline and acidic media, using cerium(IV) sulfate as ceria precursor and cetyltrimethylammonium tosylate as template, in order to evaluate the effect of pH on the morphology and texture of synthesized materials. The results show that the surface area, the pore size and volume, and the surface charge can be tuned by changing the pH. Both ceria materials are formed by nanoparticles although in the material synthesized in acidic media ($CeO_2$(B)) the particles tend to form an ordered mesoporous structure with a narrower porous size distribution, mainly due to the formation of voids between them. $CeO_2$ material synthesized in alkaline media ($CeO_2$(A)), on the contrary, shows an irregular distribution of the pores with different sizes, which were probably formed by the stacking of ceria particles. These differences seem to be also attributed to the interaction between CTAT and ceria nanoparticles during the synthesis at both experimental conditions. The grain size, the surface area, the porous volume, and the isoelectric point of the synthesized materials were 8.5 nm, 33.52 $m^2\ g^{-1}$, 0.06 $cm^3\ g^{-1}$, and 4 for $CeO_2$(A), respectively; and 13.4 nm, 21.98 $m^2\ g^{-1}$, 0.05 $cm^3\ g^{-1}$, and 7.4 for $CeO_2$(B), respectively. Adsorption studies of synthesized materials toward tetracycline and minocycline antibiotics were performed and discussed.



## 1. Introduction

Cerium(IV) oxide or ceria, $CeO_2$, is a cubic fluorite-type oxide in which each cerium site is surrounded by eight oxygen sites in fcc arrangement and each oxygen site has a tetrahedron cerium site. It is considered as the most important of rare-earth oxide, due to extraordinary thermal and chemical stability, which makes the system promising for many application patents [1]. The high level of interest is due to important industrial applications such as solid oxide fuel cells, insulators, high refractive index materials, UV filters, polishing materials, gas sensors, high-temperature oxidation resistance, free-radical scavengers, etc. [1–6]. Recently, Asati et al. [7] showed that $CeO_2$ nanoparticles have a great potential as antioxidant and radioprotective agents for applications in cancer therapy. The use of $CeO_2$ as catalysts and adsorbents has been also reported. However, most of the experimental and theoretical studies are focused in removal gas-phase adsorbates, e.g. CO and NO, from the catalytic application and those related to automobile toxic emission control points of view [8–10]. Works about removal aqueous adsorbates of environmental concern are less published and they need further investigation. In recent years, Ji et al. [11] reported the adsorption and photodegradation of the azodye acid orange 7 (AO7) on the surface of $CeO_2$. The authors showed a strongly adsorption of AO7 in the pH range between 2.96 and 4.50 at room temperature although it decreases as pH increases. The adsorption mechanism is related to a Lewis acid–base reaction which implies the formation of an inner-sphere complex. Other works revealed that $CeO_2$ can maintain the excellent adsorption capacity at temperatures as high as 800 °C under some specific conditions [12,13], and that the presence of common anions such as nitrate, chloride, sulfate, and carbonate in aqueous solution has no significant impact on its adsorption ability [14,15].

$CeO_2$ can be commercially obtained or it can be synthesized in a laboratory with a desired structure by using cerium(III and/or IV) inorganic salts as ceria precursors [1]. Numerous techniques, such as hydrothermal [16], sonochemical [17], pyrolysis [18], sol–gel [19], microwave [20] and homogeneous precipitation [21] among others have been proposed for the synthesis of not only pure ceria but also of doped and mixed cerias, with promising control of material properties. Some of them have been carried out in colloidal systems, such as emulsions and microemulsions, ionic liquids, or in the presence of surfactants and polymers aiming to enhance physical or chemical properties such as morphology, surface area, sintering resistance, activity toward a certain reaction, etc. [1,22].

Many research groups have investigated different surfactant-ceria chemistry systems that yield various shapes including

* Corresponding author. Tel.: +54 291 4595101x3523.
*E-mail address:* brigante@uns.edu.ar (M. Brigante).

1385-8947/$ – see front matter © 2012 Elsevier B.V. All rights reserved.
doi:10.1016/j.cej.2012.02.064

mesoporous structures [2], thin films [23], nanorods [24], and nanowires [25]; nanopolyhedra [26]; nanospheres [27]; and so on, depending on the synthesis conditions. The pH of the reaction medium is also a significant parameter affecting the nature and crystallinity of the synthesized materials. In this sense, Wu et al. [28] reported on the effects of pH of the reaction medium on the crystallization of ceria grains under hydrothermal conditions when cerium hydroxide was used as the precursor. The authors showed that the synthesis mechanism was by Ostwald ripening, where in an acidic medium and with the dissolution of the precursor, grain growth is faster in contrast to a basic medium. Recently, we have reported that the morphology and the pore size of mesoporous silicas, synthesized by a hydrothermal method using the cationic surfactant cetyltrimethylammonium tosylate (CTAT) as template, can be tuned by changing the pH [29]. In fact, microscopic bicontinuous materials are obtained in alkaline synthesis while monolithic silicas are obtained in acidic synthesis.

Taking into account the mentioned above, the aim of this article is divided in two parts. First, to present a study of the synthesis of $CeO_2$ by a simple and inexpensive method, using cerium(IV) sulfate as ceria precursor and CTAT as template, and evaluating the effect of the pH on the morphology and texture of the synthesized materials. This ceria precursor was chosen because it appears more suitable for forming $CeO_2$ nanoparticles at room temperature in comparison with other inorganic cerium salts such as cerium(III) nitrates [30]. The second part involves the study of the adsorption kinetics of two antibiotics on the synthesized materials in order to evaluate them as decontaminant from industrial wastewaters. Tetracycline (TC) and minocycline (MC) were used for those proposes. Both are antibiotics from tetracycline's family that exhibit broad-spectrum antimicrobial activities against a variety of disease producing bacteria. The maximum permissible concentration of TC (and MC) in aqueous solutions for industrial and pharmacy wastewaters is very low ($1\,\mu g\,L^{-1}$) although concentrations of $15\,\mu g\,L^{-1}$ in wastewater effluents have been reported [31]. It is known that the studied antibiotics are not stable at long times. In fact, TC fastly decomposes in aqueous solutions and in presence of $TiO_2$-based catalyst dispersions under UV light [32]. However, it is also known that exposures to residues of their transformed products might cause a variety of adverse effects, including acute and chronic toxicity, and microorganism antibiotic resistance [33,34]. This, together with the frequent detection of tetracycline antibiotics and its metabolites in surface, ground, and waste waters attracts our attention to the study of the antibiotic–adsorbent interactions and to the use of new materials for pollution control.

## 2. Materials and methods

### 2.1. Chemicals

Cetyltrimethylammonium *p*-toluene sulfonate or tosylate (CTAT, MW = 455.7 g mol$^{-1}$) was obtained from Aldrich. Cerium(IV) sulfate were purchased from BDH Reagents & Chemicals. HCl, NaOH, KCl, $KNO_3$, HCl, $HNO_3$, sodium acetate, and acetic acid were obtained from Anedra. Minocycline and tetracycline hydrochloride were purchased from PARAFARM, and its purity (99%) was confirmed by X-ray diffraction (XRD) and FT-IR spectroscopy. All chemicals were of analytical grade and used as received. Doubly distilled water was used for the preparation of solutions.

TC and MC present different ionic states depending on the solution pH as shown in Fig. 1. The fully protonated species of TC ($TCH_3^+$) which exists at pH < 3 [35,36] is shown in Fig. 1a. As the pH increases, the first deprotonation step ($pK_a = 3.3$) occurs at the hydroxyl group on C3 leading to the formation of a zwitterion ($TCH_2^{\pm}$) with a positive charge located on the protonated dimethylammonium group and a negative charge delocalized over the A ring. The second deprotonation step ($pK_a = 7.7$) takes place in the diketone system involving O11 and O12 generating a species with negative net charge ($TCH^-$). Finally, the third deprotonation ($pK_a = 9.5$) involves the dimethylamino group giving rise to species with two negative charges ($TC^{2-}$). On the contrary, MC has four $pK_a$ values [35,36]. The fully protonated species of MC which exists at low pH values ($MCH_4^{2+}$) is shown in Fig. 1b. As the pH increases, the first deprotonation step ($pK_a = 2.8$) occurs at the hydroxyl group on C3 leading to the formation of a species with one positive charge ($MCH_3^+$). The second deprotonation step ($pK_a = 5.0$) takes place in the aromatic amino group generating a zwitterionic species ($MCH_2^{\pm}$). The third deprotonation ($pK_a = 7.8$) involves the O10–O12 ketophenolic hydroxyl group giving rise to a species with negative charge ($MCH^-$). Finally, the fourth deprotonation ($pK_a = 9.5$) involves the dimethylamino group giving rise to a species with two negative charges ($MC^{2-}$).

### 2.2. Synthesis and characterization of $CeO_2$

Ceria was synthesized in alkaline medium as follows: 40 mL of CTAT solution was prepared by adding 0.261 g of the surfactant to water. Then, 20 mL of NaOH 1.375 M was added to the surfactant solution under vigorous stirring. To obtain the material 1 g cerium(IV) sulfate was added 15 min after the addition of the NaOH solution. The resulting product was stirred for 30 min at 500 rpm and then left for 24 h at room temperature. Then, it was filtered and washed with distilled water and left to dry at room temperature. Finally, it was calcined in an air flux by increasing the temperature from room temperature to 540 °C with a heating rate of 2 °C min$^{-1}$, and holding for 7 h at 540 °C. The obtained material was named $CeO_2$(A) and its final molar gel composition was: 1 $Ce(SO_4)_2$:0.19 CTAT:9.14 NaOH:1107 $H_2O$.

The synthesis of the mesoporous silica in acidic medium was carried out in similar conditions as described above except that the NaOH solution was substituted by 20 mL of HCl 1.375 M. The obtained material was named $CeO_2$(B).

The synthesized $CeO_2$ were characterized by the techniques usually employed in porous materials, such as scanning and transmission electron microscopy; XRD; FT-IR spectroscopy; electrophoretic mobility measurements; and the $N_2$-BET method for surface area, pore volume and pore diameter determination. Scanning electron microscopy (SEM) was performed using an EVO 40-XVP microscope. The samples were prepared on graphite stubs and coated with a ca. 300 Å gold layer in a PELCO 91000 sputter coater. Transmission electron microscopy (TEM) was performed using a JEOL 100 CX II transmission electron microscope, operated at 100 kV with magnification of 450,000×. Observations were made in a bright field. The powdered samples were placed on cooper supports of 2000 mesh. XRD patterns were collected via a Philips PW 1710 diffractometer with Cu Kα radiation (λ = 1.5406 Å) and graphite monochromator operated at 45 kV, 30 mA and 25 °C. The isoelectric point (IEP) of $CeO_2$ samples was measured with a Zetasizer Nano Series instrument (Malvern Instruments Ltd.) at room temperature. Stock $CeO_2$ suspensions containing 0.1 g L$^{-1}$ of solid in $10^{-2}$ M $KNO_3$ were used for those purposes. The pH of the suspensions was then adjusted to the desire value by adding small volumes of $HNO_3$ or KOH solutions. The $N_2$ adsorption isotherms at 77.6 K were measured with a Quantachrome Nova 1200e instrument. Each sample was degassed at 373 K for 720 min at a pressure of $1 \times 10^{-4}$ Pa. FT-IR experiments were recorded in a Nicolet FT-IR Nexus 470 Spectrophotometer. To avoid co-adsorbed water, the samples were dried under vacuum until constant weight was achieved and diluted with KBr powder before the FT-IR spectrum was recorded.

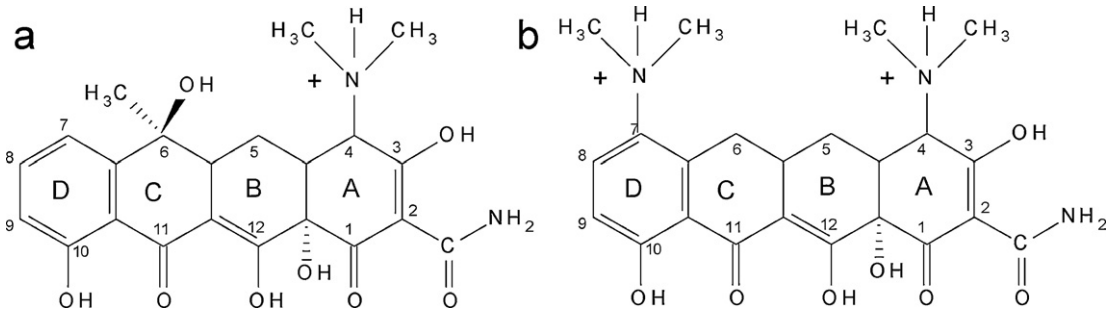


**Fig. 1.** Molecular structure of fully protonated tetracycline (a) and minocycline (b).

### 2.3. Adsorption experiments

Adsorption experiments (in darkness to avoid photodegradation) were obtained with a batch kinetic procedure using a 15 mL polypropylene centrifuge tube covered with a polypropylene cap immersed in a thermostatic shaker bath. Before starting the experiment, stock TC and MC solutions ($5 \times 10^{-4}$ M) were prepared by adding the corresponding solid to pH buffer solutions. The pHs used in these studies were 4.4 by using a 0.1 M acetate/acetic acid buffer solution. 50 mg of mesoporous material were introduced into the tubes and mixed with varying quantities of TC (or MC) and KCl (used as supporting electrolyte) solutions. The range of initial antibiotic concentration was 5–400 μM, and the final volume was 8 mL. The stirring rate was kept constant at 90 rpm. At different reaction times, the particles were separated from the supernatant by centrifugation at 4000 rpm during 2 min and the supernatant was immediately analyzed to quantify the concentration of adsorbed antibiotic. After the quantification (see below), that took around 30 s, the supernatant was reintroduced into the tube. This procedure (separation, quantification of the antibiotic and reintroduction of the supernatant into the reaction tube) was repeated during several hours in order to achieve complete adsorption of the antibiotic or to gather enough data points. The amount of adsorbed TC or adsorbed MC was calculated as the difference between the initial TC or MC concentration and the concentration of the antibiotic that remained in the supernatant solution. In most experiments no supporting electrolyte was used and the working temperature was $25.0 \pm 0.2$ °C.

Quantification of TC and MC was performed by UV–vis spectroscopy at 358 and 354 nm for pH 4.4, respectively; at 354 and 345 nm for pH 7, respectively; and at 377 nm and 382 nm for pH 9.5, respectively, using an Agilent 8453 UV–vis diode array spectrophotometer equipped with a Hellma 1 cm quartz cell. This is due to the shifting of the maximum absorption band of the antibiotics as pH varies. The supernatant of the withdrawn aliquot was placed into the cell and the spectrum was recorded in the 200–900 nm wavelength range. Calibration curves at the working pH were also constructed with several TC (and MC) solutions having concentration that ranged between $5 \times 10^{-6}$ and $1 \times 10^{-3}$ M. Very good linearity was found in all cases ($r^2 > 0.998$).

The adsorption kinetics is traditionally described following the expressions of the pseudo-first and the pseudo-second order equations originally given by Lagergren, which are special cases for the general Langmuir rate equation [37]. The pseudo-second order model, described by Eq. (1), was used here and in most solid/solution interaction studies [38]:

$$\frac{t}{q_t} = \frac{1}{k_{2,s} q_e^2} + \frac{1}{q_e} t \quad (1)$$

where $k_{2,s}$ is the pseudo-second-order rate constant ($g\,\mu mol^{-1}\,min^{-1}$); and $q_e$ and $q_t$ ($\mu mol\,g^{-1}$) denote the amount of antibiotic adsorbed at equilibrium and at the reaction time $t$, respectively. The fitting validity of this model is traditionally checked by the linear plots of $t/q_t$ versus $t$. The slope and intercept of the obtained straight line provide the respective kinetic constant and the $q_e$ parameter.

## 3. Results and discussion

### 3.1. Characterization of $CeO_2$

Fig. 2 shows the electronic micrographs of synthesized samples. According to the SEM images, $CeO_2$(A) (Fig. 2a) shows randomly shaped aggregates of variable sizes, which is probably due to a faster condensation of ceria during calcination, and these do not provide a clear morphology. The aggregates are formed by nanoparticles whose average diameter was around 9 nm (Fig. 2b), which is in agreement with those reported in literature [26]. Fig. 2b also shows that the nanoparticles are nearly spherical, but have slight faceting indicating the possibility that different crystallographic planes, each with a different atomic density, are interfacing with the aqueous phase [26]. $CeO_2$(B) particles also show randomly shaped aggregates (Fig. 2c). However, the aggregates seem to have a mesoporous structure, mainly formed by accumulation of nanoparticles whose diameter was between 10 and 13 nm, such as shown in the particle size distribution plot in the Supporting Material, SM (see SM Fig. S1).

Supplementary material related to this article found, in the online version, at doi:10.1016/j.cej.2012.02.064.

Fig. 3 shows the X-ray diffractograms of synthesized materials. Both samples show typical ceria XRD patterns at around $2\theta = 28.6$, 33.2, 47.4, 56.4, 59.1, 69.4, 76.8 and 79.1 (Fig. 3a), which are characteristic of the cubic fluorite structured $CeO_2$ [20]. The strong and sharp diffraction peaks indicate the good crystallization of the samples. No additional peaks in the XRD were observed, revealing the high purity of the prepared ceria particles. In fact, the grain size of $CeO_2$(A) nanoparticles, $D_{hkl}$, determined from the width at half maximum of the (1 1 1) peak according to the Scherrer formula [39], is 8.5 nm, which is consistent with the TEM studies. The grain size of $CeO_2$(B) was higher (13.4 nm). On the contrary, and based on the fact that the diffraction peaks at 1–5° in the XRD pattern of prepared $CeO_2$ have not been observed, it can be concluded that the mesopores in $CeO_2$(B) are mainly formed by the accumulation of nanoparticles [2,40]. Table 1 summarizes the characteristics of the nanoceria samples obtained from XRD patterns.

**Table 1**
The characteristics of the nanoceria samples from XRD patterns.

| Sample | $D_{hkl}$ (nm) | $2\theta$ | Lattice parameter (Å) | Cell volume (Å$^3$) |
|---|---|---|---|---|
| $CeO_2$(A) | 8.5 | 28.559 | 3.123 | 30.459 |
| $CeO_2$(B) | 13.4 | 28.440 | 3.136 | 30.835 |

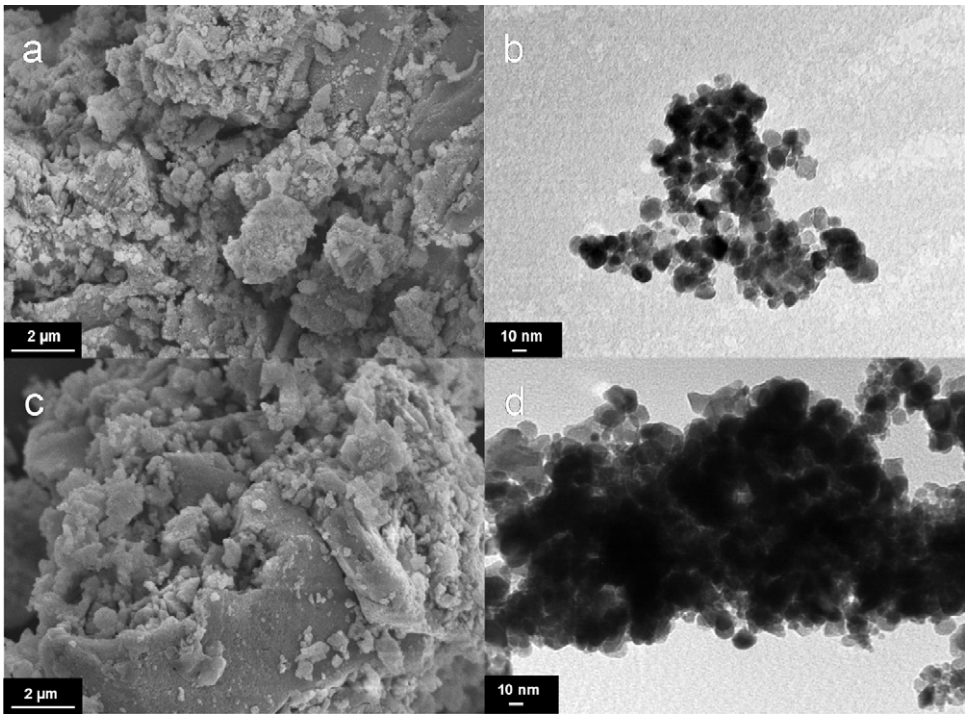


**Fig. 2.** SEM (20,000×, left side) and TEM (450,000×, right side) micrographs of: (a and b) $CeO_2$(A), and (c and d) $CeO_2$(B).

Differences in morphology and texture between $CeO_2$(A) and $CeO_2$(B) are not only attributed to the pH synthesis but also to the interaction between the template and the ceria particles during the synthesis. Cationic surfactants are expected to be favorably adsorbed on ceria nanoparticles, primarily due to the high electronegativity of the oxygen atoms of ceria, preventing van der Waals' driven agglomeration or ripening by terminating the nanoparticle growth [1]. This interaction is also favored by increasing the pH of the synthesis medium, mainly due the higher availability of surface OH groups [1]. At alkaline pH, the positive interaction between CTAT and $CeO_2$ tends to form more dispersed nanoparticles, as shown in the TEM micrograph of $CeO_2$(A) (Fig. 2b). At acidic pH, on the contrary, the lower interaction between the surfactant and $CeO_2$(B) tends to form a mesopore structure by agglomeration of ceria particles, as shown in Fig. 2d. The effect of preventing agglomeration of particles by cationic surfactants was also reported by Mehta et al. [41] on the synthesis of ZnS nanoparticles in presence of cetyltrimethylammonium chloride and cetyltrimethylpyridinium chloride.

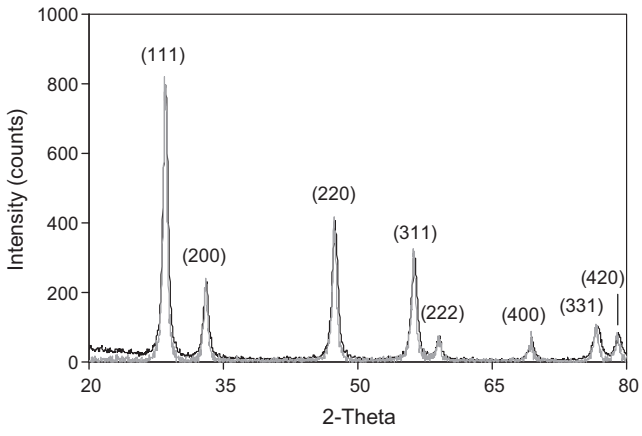


**Fig. 3.** XRD patterns of synthesized $CeO_2$(A) (black) and $CeO_2$(B) (grey).

Nitrogen sorption isotherms of $CeO_2$ materials are shown in Fig. 4. $CeO_2$(A) (Fig. 4a) exhibits a type IV isotherm with a H3 hysteresis loop that is characteristic of porous materials [20]. The BET surface area and the pore volume were calculated to be 33.52 $m^2\,g^{-1}$ and 0.06 $cm^3\,g^{-1}$, respectively. The BJH pore size distribution (inset in Fig. 4a) shows an irregular distribution of the pores in the material. In the range of 1.50–60.00 nm, there were two peaks at 2.02 nm and 12.92 nm. This irregularity suggests the co-existence of pores with different sizes, which were probably formed by the stacking of $CeO_2$ particles [22]. $CeO_2$(B) also shows a type IV isotherm but with a H1 hysteresis loop (Fig. 4b), typical of agglomerates of particles or meporous materials with cylindrical or rod-like geometry of the pores [42]. The surface area and pore volume were lower than ceria synthesized at alkaline pH, i.e., 21.98 $m^2\,g^{-1}$ and 0.05 $cm^3\,g^{-1}$, respectively. This is mainly due to the formation of higher size particles that decrease the adsorption active sites for $N_2$. The well-defined step which occurs at relative high pressure of 0.8–1.0, corresponding to capillary condensation of $N_2$, indicates the uniformity of the pores, which are constituted by the voids between primary particles [43]. In fact, the pore size was sharply distributed in a narrow range centered at approximately 6.0 nm (inset in Fig. 3b).

The variation of the zeta potential as a function of the pH and the FT-IR spectra of synthesized materials are shown in Fig. 5. $CeO_2$(A) nanoparticles have an isoelectric point of 4.0 (Fig. 5a), which values are closed with the results recently reported by Goharshadi et al. [20] on the synthesis of $CeO_2$ nanoparticles obtained by a microwave method, respectively. $CeO_2$(B), on the contrary, has an IEP of 7.4 which is similar to those reported by Buettner et al. [26] on the synthesis of ceria nanoparticles by precipitation using cerium(III) nitrate, $NH_4OH$ and water. The difference in the IEP values is strongly related to the synthesis method and the chemicals

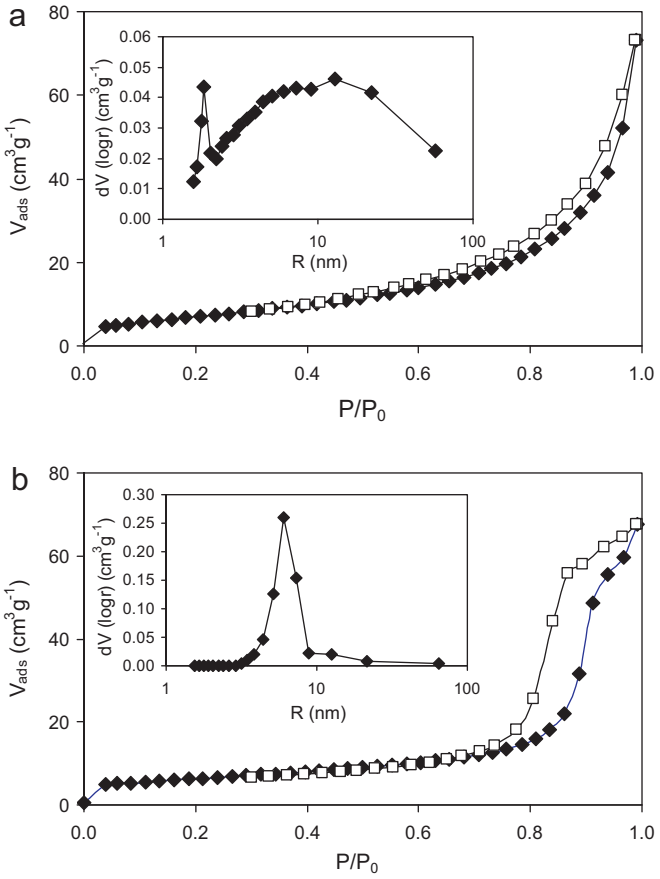


**Fig. 4.** Nitrogen adsorption (solid symbols)–desorption (open symbols) isotherms on (a) $CeO_2$(A), and (b) $CeO_2$(B). The inset of both figures shows the pore radius distribution.

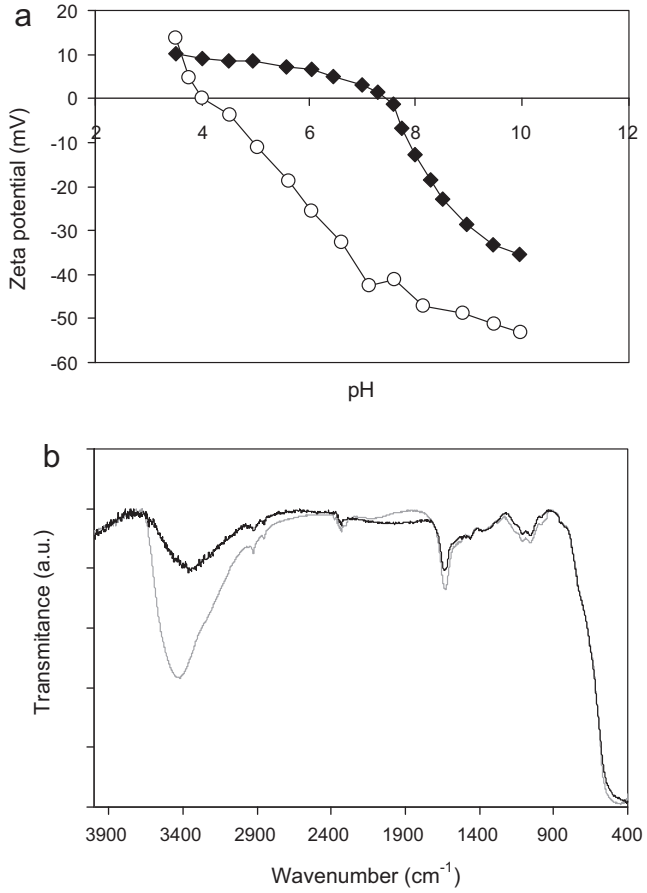


**Fig. 5.** (a) Electrophoretic mobilities of the studied samples as a function of pH in $10^{-3}$ M $KNO_3$ solutions: open circles, $CeO_2$(A); and solid diamonds, $CeO_2$(B). (b) Infrared spectra of $CeO_2$(A) (black) and $CeO_2$(B) (grey).

involved in the synthesis, i.e. NaOH and HCl. In fact, Patil et al. [44] reported that the use of $NH_4OH$ for the synthesis of $CeO_2$ by microemulsion process leads a material with an IEP of 4.5 whereas the ceria nanoparticles treated with a HCl solution in the last step during hydrothermal synthesis process leads a material with an IEP of 9.5. Fig. 5b shows the FT-IR spectra of $CeO_2$(A) and $CeO_2$(B). The most important features of both materials are a broad band centered at around 3450 $cm^{-1}$ related to O—H stretching frequency, a peak located at around 1640 $cm^{-1}$ due to the bending vibration of associated water, and a peak centered at 447 $cm^{-1}$ which are attributed to Ce—O stretching [45]. The vibration peaks located between 980 and 1250 $cm^{-1}$ are similar to that of commercial ceria powders [46] and those reported by Li et al. [40] on the synthesis of 3D flowerlike $CeO_2$ microspheres. Xu et al. [30] assigned this band to the vibration modes of $SO_4^{2-}$. These sulfate species are coordinated with unsaturated surface $Ce^{4+}$ cations and therefore may have the potential in acting as the superacid centers for certain catalytic reactions [30]. Fig. 5a also shows that the band located at around 3445 $cm^{-1}$ is broader and more intense in ceria synthesized in acidic pH. On the contrary, this band is commonly associated to physically adsorbed water but it can also referred to surface OH [45,47], which suggests that $CeO_2$(B) would have a major content of hydroxyl surface groups in comparison of $CeO_2$(A). On the contrary, it is known that ceria surface has both Lewis and Bronsted acid sites [48]. Therefore, the differences in intensity of the 3445 $cm^{-1}$ band can be also attributed to differences in Lewis/Bronsted sites ratio. Both suggestions can modify not only the surface charge development as a function of pH of studied solids but also their adsorption properties.

### 3.2. MC adsorption studies

The adsorption kinetic of TC and MC on both $CeO_2$ materials at pH 4.4 and 25 °C was shown in Fig. 6. The adsorption of both antibiotics is very fast between $t = 0$ and $t = 5$ min (Fig. 6a). It is so fast that no data point could be measured in this period with our experimental set up. At $t > 5$ min the adsorption takes place at a much slower and measurable rate. Although adsorption seems to reach completion at around 240 min, some long-term kinetic experiments revealed that adsorption continues after several days, but very slowly. Fig. 6a also shows that the adsorption on both adsorbents is strongly dependent on the synthesis pH and the nature of the antibiotic. On the contrary, the adsorption of MC was higher than of TC. At pH 4.4, MC forms a monovalent cation whereas TC is mainly present as a zwitterionic. Therefore, the interaction between MC (as $MCH_3^+$) and the ceria functional groups, mainly driven by electrostatic interactions and H-bonds formations, is higher than in TC (as $TCH_2^{\pm}$) and ceria. Such interactions, mainly between dimethylamino, amide, carbonylic and phenolic groups of the antibiotic and the functional groups of $CeO_2$ nanoparticles, were supported in a recent paper, where the effect of the pH, temperature and ionic strength on the adsorption of MC on $CeO_2$(A) were evaluated [49]. On the contrary, the adsorption capacity in $CeO_2$(B) is higher than in $CeO_2$(A). At the beginning, we would have expected the opposite, i.e., $CeO_2$(A) > $CeO_2$(B), mainly due to: (a) the higher surface area, which increases the active sites; and (b) the negative charge at the studied pH (IEP = 4), which promotes the electrostatic attraction between the antibiotics and the surface. However, the higher adsorption in $CeO_2$ synthesized in acidic medium seems to

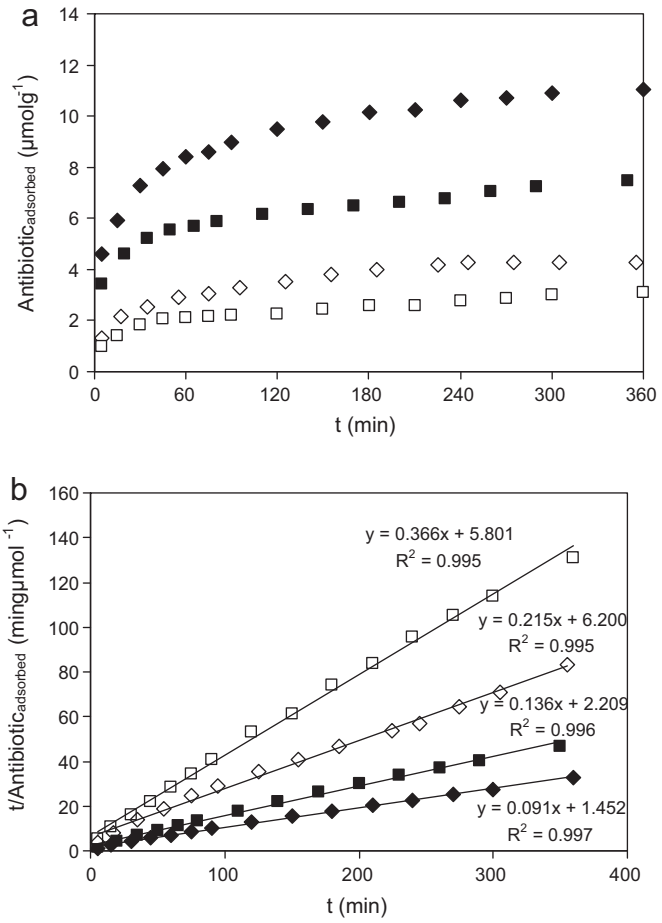


**Fig. 6.** (a) Adsorption kinetics of TC (squares) and MC (diamonds) on the studied materials at pH 4.4 and 25 °C. (b) Fitting the experimental data by using Eq. (1). Open symbols, $CeO_2$(A); and solid symbols, $CeO_2$(B).

be related to its mesoporous structure, which favors the diffusion of the adsorbate and the interaction with the pore walls; and/or the change in the interaction mode between the adsorbates and the adsorbent. That is, electrostatic attractions and H-bond formations are also expected in $CeO_2$(B) although other type of interactions, such as ion-exchange and hydrophobic interactions, should be also taken into account at pH 4.4 due to its surface charge development (at pH 4.4 the surface is positively charged). Similar suggestions were reported by other authors on the adsorption of tetracycline antibiotics on several adsorbents [50,51].

MC and TC adsorption on $CeO_2$ seems to take place by binding the antibiotics to the ceria generating surface species TC–$CeO_2$ and MC–$CeO_2$. The binding between the antibiotic and ceria can be visualized comparing the FT-IR spectra of pure MC, and MC adsorbed on $CeO_2$(A) and $CeO_2$(B) at pH 4.4 such as shown in Fig. 7. MC (and TC) shows characteristic peaks at 2743 cm$^{-1}$ and 2657 cm$^{-1}$ associated to $NHR_3^+$ group, 1674 cm$^{-1}$ (1657 cm$^{-1}$) and 1520 cm$^{-1}$ (1516 cm$^{-1}$) assigned to the Amide I and Amide II bands, 1615 cm$^{-1}$ (1595 cm$^{-1}$) and 1582 cm$^{-1}$ (1569 cm$^{-1}$) assigned to C=O stretching vibration at rings A and C respectively, 1456 cm$^{-1}$ (1458 cm$^{-1}$) assigned to C—C stretching vibration, 1378 cm$^{-1}$ (1380 cm$^{-1}$) assigned to $-CH_3$ deformation vibration, 1247 cm$^{-1}$ which is attributed to C—N amine stretching vibration, and 1176 cm$^{-1}$ assigned to the phenolic C—O stretching band [52,53]. In parentheses are listed some of the calculated peak position of tetracycline antibiotics obtained by Leypold et al. [53] via DFT calculations. Ceria peaks were observed in the IR spectra of MC–$CeO_2$(A) and MC–$CeO_2$(B) (the band at 1640 cm$^{-1}$, due to the bending vibration

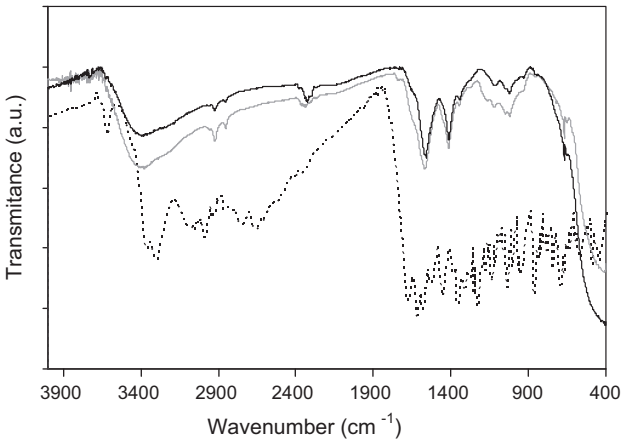


**Fig. 7.** Infrared spectra of MC (dotted), MC–$CeO_2$(A) (black) and MC–$CeO_2$(B) (grey).

of associated water, appears now as a shoulder), whereas the bands assigned to $NHR_3^+$ group were not observed. The peaks assigned to the polar groups of the antibiotics were shifted to lower frequencies with respect to bulk antibiotic. Similar results were found in the TC–$CeO_2$ systems (data not shown) and those reported by Parolo et al. [35] in the TC and MC–montmorillonite systems. The obtained results show that the $NHR_3^+$ groups of both antibiotic are bound to the ceria surface, mainly due to electrostatic interactions, whereas other polar groups of the molecule could participate in non-electrostatic interactions (e.g. H-bond formations) with the surface. As mentioned above, hydrophobic interactions between the antibiotics and positively charged surface of $CeO_2$(B) should be also taken into account.

All data were well-fitted to the pseudo-second order equation with $r^2 > 0.995$ as shown in Fig. 6b. Even though the formulated model is rather simple, it can fit reasonably well the adsorption behavior of studied antibiotics. The $q_e$ and $k_{2,s}$ values for TC and MC adsorption on $CeO_2$(A) at pH 4.4 were $5.12 \times 10^{-3}$ and $7.46 \times 10^{-3}$ g μmol$^{-1}$ min$^{-1}$, respectively. The $k_{2,s}$ values for TC and MC adsorption on $CeO_2$(B) at the same pH were $8.39 \times 10^{-3}$ and $6.49 \times 10^{-3}$ g μmol$^{-1}$ min$^{-1}$, respectively. These values are comparable to those reported in a previous paper on the adsorption of TC on $TiO_2$ nanoparticles and on the binary system $TiO_2$–$SiO_2$ at the same experimental conditions [32] suggesting that ceria materials can act as a good adsorbent for tetracycline antibiotics kinetically.

## 4. Conclusions

The results shown in this article reveal that the surface area, pore size and volume, and surface charge development as a function of pH of studied solids are strongly dependent on the pH synthesis. Both ceria materials are formed by nanoparticles although in the material synthesized in acidic media the particles tend to form a mesoporous structure with a narrower porous size distribution, mainly due to the formation of voids between them. $CeO_2$ synthesized in alkaline media, on the contrary, shows an irregular distribution of the pores with different sizes, which were probably formed by the stacking of ceria particles. The grain size, the surface area, the porous volume, and the isoelectric point of the synthesized materials were 8.5 nm, 33.52 m$^2$ g$^{-1}$, 0.06 cm$^3$ g$^{-1}$, and 4 for $CeO_2$(A), respectively; and 13.4 nm, 21.98 m$^2$ g$^{-1}$, 0.05 cm$^3$ g$^{-1}$, and 7.4 for $CeO_2$(B), respectively. The adsorption capacities of studied materials toward tetracycline and minocycline are also different, i.e., the adsorption of tetracycline and minocycline on $CeO_2$(A) is lower than on $CeO_2$(B). The adsorption is strongly related to electrostatic interactions and H-bond formations mainly between functional groups of the antibiotic drug and $CeO_2$, although other

interactions, such as hydrophobic interactions, might be also present, mainly in $CeO_2$(B).

The obtained results have a significant importance in several processes, where the control of the pH (within others variables) in the production of synthetic materials can play a key role. Taking into account this concept, one can design a convenient and economic path for getting the mesoporous products to match the desired applications. Based on our results, $CeO_2$ materials synthesized at alkaline pH have higher surface area and lower IEP than at acidic pH, which would be desirable in the remotion of several heavy metals and other cationic species. On the contrary, ceria synthesized in acidic media is positively charged at neutral pH, which would be desirable in, for example, the remotion of polar and anionic-type pollutants from industrial wastewaters.

## Acknowledgments

This work was financed by SECyT-UNS, CONICET and ANPCYT. The authors thank Olga Pieroni (Departamento de Química, UNS) and Leticia Lescano (Departamento de Geología, UNS) for the FT-IR spectra and X-ray diffractograms, respectively. M. Brigante thanks CONICET for the postdoctoral fellowship.

## References

[1] A. Bumajdad, J. Eastoe, A. Mathew, Cerium oxide nanoparticles prepared in self-assembled systems, Adv. Colloid Interface Sci. 147 (2009) 56–66.
[2] I.M. Hung, H.P. Wang, W.H. Lai, K.Z. Fung, M.H. Hon, Preparation of mesoporous cerium oxide templated by tri-block copolymer for solid oxide fuel cell, Electrochim. Acta 50 (2004) 745–748.
[3] P. Chen, S. Patil, S. Seal, J.F. McGinnis, Rare earth nanoparticles prevent retinal degeneration induced by intracellular peroxides, Nat. Nanotechnol. 1 (2006) 142–150.
[4] J. Niu, A. Azfer, L.M. Rogers, X. Wang, P.E. Kolattukudy, Cardioprotective effects of cerium oxide nanoparticles in a transgenic murine model of cardiomyopathy, Cardiovasc. Res. 73 (2007) 549–559.
[5] T.S. Stefanik, H.L. Tuller, Ceria-based gas sensors, J. Eur. Ceram. Soc. 21 (2001) 1967–1970.
[6] M. Yamashita, K. Kameyama, S. Yabe, S. Yoshida, Y. Fujishiro, T. Kawai, T. Sato, Synthesis and microstructure of ceria doped ceria as UV filters, J. Mater. Sci. 37 (2002) 683–687.
[7] A. Asati, S. Santra, C. Kaittanis, J.M. Perez, Surface-charge-dependent cell localization and cytotoxicity of cerium oxide nanoparticles, ACS Nano 9 (2010) 5321–5331.
[8] B. Azambre, L. Zenboury, F. Delacroix, J.V. Weber, Adsorption of NO and $NO_2$ on ceria–zirconia of composition $Ce_{0.69}Zr_{0.31}O_2$: a DRIFTS study, Catal. Today 137 (2008) 278–282.
[9] M. Huang, S. Fabris, CO adsorption and oxidation on ceria surfaces from DFT + U calculations, J. Phys. Chem. C 112 (2008) 8643–8648.
[10] B. Azambre, L. Zenboury, A. Koch, J.V. Weber, Adsorption and desorption of NOx on commercial ceria-zirconia ($Ce_xZr_{1-x}O_2$) mixed oxides: a combined TGA, TPD-MS, and DRIFTS study, J. Phys. Chem. C 113 (2009) 13287–13299.
[11] P. Ji, J. Zhang, F. Chen, M. Anpo, Study of adsorption and degradation of acid orange 7 on the surface of $CeO_2$ under visible light irradiation, Appl. Catal. B: Environ. 85 (2009) 148–154.
[12] H. Guo, W. Li, H. Wang, J. Zhang, Y. Liu, Y. Zhou, A study of phosphate adsorption by different temperature treated hydrous cerium oxides, Rare Met. 30 (2011) 58–62.
[13] M. Flytzani-Stephanopoulos, M. Sakbodin, Z. Wang, Regenerative adsorption and removal of $H_2S$ from hot fuel gas streams by rare earth oxides, Science 312 (2006) 1508–1510.
[14] M.J. Haron, F. Ab Rahim, A.H. Abdullah, M.Z. Hussein, A. Kassim, Sorption removal of arsenic by cerium-exchanged zeolite P, Mater. Sci. Eng. B 149 (2008) 204–208.
[15] Y. Zhang, M. Yang, X. Huang, Arsenic(V) removal with a Ce(IV)-doped iron oxide adsorbent, Chemosphere 51 (2003) 945–952.
[16] A.I.Y. Tok, F.Y.C. Boey, Z. Dong, X.L. Sun, Hydrothermal synthesis of $CeO_2$ nanoparticles, J. Mater. Proc. Technol. 190 (2007) 217–222.
[17] J.C. Yu, L. Zhang, J. Lin, Direct sonochemical preparation of high-surface-area nanoporous ceria and ceria–zirconia solid solutions, J. Colloid Interface Sci. 260 (2003) 240–243.
[18] H. Oh, S. Kim, Synthesis of ceria nanoparticles by flame electrospray pyrolysis, J. Aerosol Sci. 38 (2007) 1185–1196.
[19] N. Phonthammachai, M. Rumruangwong, E. Gulari, A.M. Jamieson, S. Jitkarnka, S. Wongkasemjit, Synthesis and rheological properties of mesoporous nanocrystalline $CeO_2$ via sol–gel process, Colloids Surf. A 247 (2004) 61–68.
[20] E.K. Goharshadi, S. Samiee, P. Nancarrow, Fabrication of cerium oxide nanoparticles: characterization and optical properties, J. Colloid Interface Sci. 356 (2011) 473–480.
[21] H.Y. Chang, H.I. Chen, Morphological evolution for $CeO_2$ nanoparticles synthesized by precipitation technique, J. Cryst. Growth 283 (2005) 457–468.
[22] S. Miao, Z. Liu, Z. Miao, B. Han, K. Ding, G. An, Y. Xie, Ionic liquid-mediated synthesis of crystalline $CeO_2$ mesoporous films and their application in aerobic oxidation of benzyl alcohol, Microporous Mesoporous Mater. 117 (2009) 386–390.
[23] M. Lundberg, B. Skårman, F. Cesar, L.R. Wallenberg, Mesoporous thin films of high-surface-area crystalline cerium dioxide, Microporous Mesoporous Mater. 54 (2002) 97–103.
[24] A. Vantomme, Z.Y. Yuan, G. Du, B.L. Su, Surfactant-assisted large-scale preparation of crystalline $CeO_2$ nanorods, Langmuir 21 (2005) 1132–1135.
[25] L. Yan, X. Xing, R. Yu, J. Deng, J. Chen, G. Liu, Facile alcohothermal synthesis of large-scale ceria nanowires with organic surfactant assistance, Physica B 390 (2007) 59–64.
[26] K.M. Buettner, C.I. Rincio, S.E. Mylon, Aggregation kinetics of cerium oxide nanoparticles in monovalent and divalent electrolytes, Colloids Surf. A 366 (2010) 74–79.
[27] D. Zhang, F. Niu, H. Li, L. Shi, J. Fang, Uniform cerianano spheres: solvothermal synthesis, formation mechanism, size-control and catalytic activity, Powder Technol. 207 (2011) 35–41.
[28] N.C. Wu, E.W. Shi, Y.Q. Zheng, W.J. Li, Effect of pH of medium on hydrothermal synthesis of nanocrystalline cerium(IV) oxide powders, J. Am. Ceram. Soc. 85 (2002) 2462–2468.
[29] M. Brigante, P.C. Schulz, Synthesis of mesoporous silicas in alkaline and acidic media using the systems cetyltrimethylammonium tosylate (CTAT)-Pluronic F127 triblock copolymer and CTAT-Pluronic F68 triblock copolymer as templates, J. Colloid Interface Sci. 369 (2012) 71–81.
[30] J. Xu, G. Li, L. Li, $CeO_2$ nanocrystals: seed-mediated synthesis and size control, Mater. Res. Bull. 43 (2008) 990–995.
[31] A. Pena, M. Paulo, L.J.G. Silva, M. Seifrtová, C.M. Lino, P. Solich, Tetracycline antibiotics in hospital and municipal wastewaters: a pilot study in Portugal, Anal. Bioanal. Chem. 396 (2010) 2929–2936.
[32] M. Brigante, P. Schulz, Remotion of the antibiotic tetracycline by titania and titania–silica composed materials, J. Hazard. Mater. 192 (2011) 1597–1608.
[33] H. Schmitt, K. Stoob, G. Hamscher, E. Smit, W. Seinen, Tetracyclines and tetracycline resistance in agricultural soils: microcosm and field studies, Microb. Ecol. 51 (2006) 267–276.
[34] L. Ji, F. Liu, Z. Xu, S. Zheng, D. Zhu, Adsorption of pharmaceutical antibiotics on template-synthesized ordered micro- and mesoporous carbons, Environ. Sci. Technol. 44 (2010) 3116–3122.
[35] M.E. Parolo, M.J. Avena, G. Pettinari, I. Zajonkovsky, J.M. Valles, M.T. Baschini, Antimicrobial properties of tetracycline and minocycline-montmorillonites, J. Hazard. Mater. 192 (2011) 1597–1608.
[36] V. Orti, M. Audran, P. Gilbert, G. Bougard, F. Bressolle, High-performance liquid chromatographic assay for minocycline in human plasma and parotid saliva, J. Chromatogr. B 738 (2000) 357–365.
[37] Y.S. Ho, G. Mc Kay, Sorption of dyes and copper ions onto biosorbents, Process Biochem. 38 (2003) 1047–1061.
[38] C.E. Zubieta, P.V. Messina, C. Luengo, M. Dennehy, O. Pieroni, P.C. Schulz, Reactive dyes remotion by porous $TiO_2$-chitosan materials, J. Hazard. Mater. 152 (2008) 765–777.
[39] H.P. Klug, L.E. Alexander, X-ray Diffraction Procedures, Wiley, New York, 1954.
[40] J. Li, G. Lu, H. Li, Y. Wang, Y. Guo, Y. Guo, Facile synthesis of 3D flowerlike $CeO_2$ microspheres under mild condition with high catalytic performance for CO oxidation, J. Colloid Interface Sci. 360 (2011) 93–99.
[41] S.K. Mehta, S. Kumar, S. Chaudhary, K.K. Bhasin, Effect of cationic surfactant head groups on synthesis, growth and agglomeration behavior of ZnS nanoparticles, Nanoscale Res. Lett. 4 (2009) 1197–1208.
[42] K.S.W. Sing, D.H. Everett, R.A.W. Haul, L. Moscou, R.A. Pierotti, J. Rouquerol, T. Siemieniewska, Reporting physisorption data for gas/solid systems with special reference to the determination of surface area and porosity, Pure Appl. Chem. 57 (1985) 603–619.
[43] W.Q. Wang, J.G. Wang, P.C. Sun, D.T. Ding, T.H. Chen, Effect of alcohol on morphology and mesostructure control of anionic-surfactant-templated mesoporous silica (AMS), J. Colloid Interface Sci. 331 (2009) 156–162.
[44] S. Patil, A. Sandberg, E. Heckert, W. Self, S. Seal, Protein adsorption and cellular uptake of cerium oxide nanoparticles as a function of zeta potential, Biomaterials 28 (2007) 4600–4607.
[45] X. Li, F. Chen, X. Lu, C. Ni, Z. Chen, Modified-EISA synthesis of mesoporous high surface area $CeO_2$ and catalytic property for CO oxidation, J. Rare Earth 27 (2009) 943–947.
[46] D.S. Zhang, H.X. Fu, L.Y. Shi, C.S. Pan, Q. Li, Y.L. Chu, W.Y. Yu, Synthesis of $CeO_2$ nanorods via ultrasonication assisted by polyethylene glycol, Inorg. Chem. 46 (2007) 2446–2451.
[47] Z. Zhang, L. Yu, W. Liu, Z. Song, Surface modification of ceria nanoparticles and their chemical mechanical polishing behavior on glass substrate, Appl. Surf. Sci. 256 (2010) 3856–3861.
[48] M.I. Zaki, M.A. Hasan, F.A. Al-Sagheer, L. Pasupulety, In situ FTIR spectra of pyridine adsorbed on $SiO_2$–$Al_2O_3$, $TiO_2$, $ZrO_2$ and $CeO_2$: general considerations for the identification of acid sites on surfaces of finely divided metal oxides, Colloids Surf. A 190 (2001) 261–274.

[49] M. Brigante, P.C. Schulz, Adsorption of the antibiotic minocycline on cerium(IV) oxide. Effect of pH, ionic strength and temperature, Microporous Mesoporous Mater., in press.
[50] P. Kulshrestha, R.F. Giese, D.S. Aga, Investigating the molecular interactions of oxyteracycline in clay and organic matter: insights on factors affecting its mobility in soil, Environ. Sci. Technol. 38 (2004) 4097–4105.
[51] C. Gu, K.G. Karthikeyan, Interaction of tetracycline with aluminum and hydrous iron oxides, Environ. Sci. Technol. 39 (2005) 2660–2667.
[52] G. Caminati, C. Focardi, G. Gabrielli, F. Gambinossi, B. Mecheri, M. Nocentini, M. Puggelli, Spectroscopic investigation of tetracycline interaction with phospholipid Langmuir–Blodgett films, Mater. Sci. Eng. C 22 (2002) 301–305.
[53] C.F. Leypold, M. Reiher, G. Brehm, M.O. Schmitt, S. Schneider, P. Matousek, M. Towrie, Tetracycline and derivatives-assignment of IR and Raman spectra via DFT calculations, Phys. Chem. Chem. Phys. 5 (2003) 1149–1157.